



This work was carried out in whole or in part within the framework of the NOMATEN Center of Excellence, supported from the European Union Horizon 2020 research and innovation programme (Grant Agreement No. 857470) and from the European Regional Development Fund via the Foundation for Polish Science International Research Agenda PLUS programme (Grant No. MAB PLUS/2018/8).

This is the manuscript submitted to: Nuclear Instruments and Methods in Physics Research Section B: Beam Interactions with Materials and Atoms, vol 540, July 2023, Pages 24-29, published on 14 April 2023 with the embargo period till: 14 April 2025.

DOI: 10.1016/j.nimb.2023.03.027

# Self-ion irradiation effects on nanoindentation-induced plasticity of crystalline iron: A joint experimental and computational study

K. Mulewska<sup>a,\*</sup>, F. Rovaris<sup>a</sup>, F. J. Dominguez-Gutierrez<sup>a,\*\*</sup>, W. Y. Huo<sup>a,b</sup>, D. Kalita<sup>a</sup>, I. Jozwik<sup>a</sup>, S. Papanikolaou<sup>a</sup>, M. J. Alava<sup>a,d</sup>, L. Kurpaska<sup>a,\*\*</sup> and J. Jagielski<sup>c,e</sup>

<sup>a</sup>NOMATEN Centre of Excellence, National Centre for Nuclear Research, ul. A. Soltana 7, Otwock, 05-400, Poland

<sup>b</sup>College of Mechanical and Electrical Engineering, Nanjing Forestry University, Nanjing, 210037, China

<sup>c</sup>Lukasiewicz Research Network Institute of Microelectronics and Photonics, Wolczynska 133, Warsaw, 01-919, Poland

<sup>d</sup>Department of Applied Physics, Aalto University, P.O. Box 11000, Aalto, 00076, Finland

<sup>e</sup>National Centre for Nuclear Research, ul. A. Soltana 7, Otwock, 05-400, Poland

## ARTICLE INFO

### Keywords:

irradiation damage  
nanoindentation  
Dislocation dynamics  
MD simulations  
3D-DDD simulations

## ABSTRACT

In this paper, experimental work is supported by multi-scale numerical modeling to investigate nanomechanical response of pristine and ion irradiated with Fe<sup>2+</sup> ions with energy 5 MeV high purity iron specimens by nanoindentation and Electron Backscatter Diffraction. The appearance of a sudden displacement burst that is observed during the loading process in the load–displacement curves is connected with increased shear stress in a small subsurface volume due to dislocation slip activation and mobilization of pre-existing dislocations by irradiation. The molecular dynamics (MD) and 3D-discrete dislocation dynamics (3D-DDD) simulations are applied to model geometrically necessary dislocations (GNDs) nucleation mechanisms at early stages of nanoindentation test; providing an insight to the mechanical response of the material and its plastic instability and are in a qualitative agreement with GNDs density mapping images. Finally, we noted that dislocations and defects nucleated are responsible the material hardness increase, as observed in recorded load–displacement curves and pop-ins analysis.

## 1. Introduction

In recent years, with the development of new experimental techniques such as nanoindentation [1, 2, 3] and pillar compression [4, 5], tens and hundreds of nanometers have become possible to be experimentally tested and analyzed. At the same time, one can observe increasing computational capacity and power, which allows for large scale simulation by using molecular dynamics (MD) [6, 7, 8, 9, 10, 11, 12, 13] or discrete dislocation dynamics (DDD) [14, 15] of larger material volumes. Combining these two routes enables us to assume that experimentally observed crystal plasticity instability can be visualized by in-situ or post-mortem transmission electron microscopy (TEM) [16, 17, 18] following dynamically the interaction of dislocations with microstructural features of the samples numerically. This offers a valuable opportunity to better understand the phenomena occurring in the tested material, their interaction, and the impact of microstructural features such as grain boundaries, grain orientation or precipitates on the mechanical properties such as hardness or yield strength [1, 8, 19, 20, 21]. Along this research line and goal, the combination of experimental and numerical tools are essential for understanding the impact of radiation damage and induced defect production [22].

The ferritic/martensitic (F/M) steels are planned to be used in Generation IV nuclear reactors. They exhibit much

lower swelling than austenitic steels, thus they can be utilized even up to 200 dpa [23]. Those materials also display desired properties: higher thermal conductivity, lower thermal expansion, and a lower tendency to He embrittlement. However, F/M steels typically display significant hardening when exposed to radiation at temperatures around 300°C, the operating temperature of most reactors. In addition, temperature fluctuations shall be unavoidable due to transients and temperature gradients (depending on reactor component particulars). Hardening is commonly caused by creation of defects that pin and block dislocation movement, typically resulting in an increase of hardness and a decrease in fracture toughness, that is caused by localization of plastic deformation, with subsequent dramatic loss of uniform elongation.

To experimentally simulate radiation defects, one can either perform neutron irradiation in the reactor core or use an ion accelerator facility and perform ion irradiation. The second option is very tempting as an ion irradiation provides an opportunity to produce controlled amounts of displacement damage under well-defined experimental conditions. It is well established that ion irradiation can reproduce all standard microstructural features observed in neutron-irradiated materials (dislocation loops, voids, and bubbles, radiation-induced solute segregation, or radiation-induced precipitates) [19, 20, 24]. Charged particle irradiation in recent years has become valuable complementary tool to bulk neutron irradiation studies [25, 26]. However, the possible length scale of the irradiation damage region usually does not exceed few  $\mu\text{m}$  for few MeV energies [27]. Despite this limitation, the development of experimental tools like high resolution scanning electron microscopy/focused ion beam

\*Principal corresponding author

\*\*Corresponding author

✉ katarzyna.mulewska@ncbj.gov.pl (K. Mulewska);

javier.dominguez@ncbj.gov.pl (F.J. Dominguez-Gutierrez);

lukasz.kurpaska@ncbj.gov.pl (L. Kurpaska)

ORCID(s): 0000-0002-0729-5409 (F. Rovaris)

(HR SEM/FIB) and TEM in the case of structural investigations or nanoindentation allows for mechanically testing sufficiently small volumes, which are relevant for ion irradiation conditions [20]. Finally, one must remember that the ion-irradiation offers opportunities for improved experimental control that is impossible to perform during reactor neutron irradiation such as separate effects testing. Therefore, the separation of different environmental conditions is much easier, hence understanding individual phenomena becomes possible. One of these phenomena is the impact of radiation defects on the dislocation nucleation process and evolution.

It has been commonly agreed that the nanoindentation method is one of the key techniques in understanding plasticity in small volumes [1, 3, 21, 28]. A common agreement has been achieved that this technique can be used to study fundamental dislocation nucleation aspects. The advantage of this technique is the ability to probe small volumes, limiting effect of different types of microstructural defects. Suppose one is testing single crystals or individual, large grains. In that case, it can be assumed that the onset of plasticity is marked by the characteristic discontinuity in the load-indentation depth (L-D) curves, called a “pop-in” event. These events are generally explained by homogeneous dislocation nucleation. It is also assumed that these effects occur when shear stress generated under the indenter tip approaches the material’s theoretical shear strength. When the first pop-in effect is observed [18], which means that the homogeneous dislocation nucleation in the defect-free (this is valid for single crystals or grains probed sufficiently far from the grain boundary) volume occurred [20]. The evolution of the dislocation can be better understood if a computational model is applied at different length-time scales. This has been well documented for face centered cubic (FCC) systems. However, dislocation motion and interaction in body centered cubic (BCC) are still poorly understood. Several features such as interstitial atoms, surface roughness, crystal orientation, or existing dislocation density and their interaction are to be explained [13]. The situation is even more complicated for the irradiated system when radiation defects are introduced to the material, and they evolve in time and scale.

Considering all the above aspects, the present paper aims to better understand the effect of incipient plasticity in BCC-type high purity Fe (model material). Our experimental and numerical studies are performed on pristine and ion-irradiated materials. We consider one-grain orientation and analyze the possible correlation between the crystallographic orientation, presence of radiation defects, and occurrence of pop-in events. We extrapolate our atomistic simulation based on molecular dynamics (MD) method by performing discrete dislocation dynamics (DDD) simulations to investigate the evolution of dislocation forest at larger material volumes during nanoindentation testing. DDD and MD simulations are both useful computational methods that can be used together to gain deeper understanding of materials behavior. DDD simulations focus on mesoscopic features of materials by modeling the movement and interactions of

dislocations, where nucleation and multiplication of dislocations is captured on the level of dislocations, but not on the atomistic scale. New dislocation segments are naturally introduced by multiplication of pre-existing dislocations. Atomistic MD simulations can guide DDD approaches by describing initial nucleation of dislocations at the onset of plasticity. Herein, the microstructure and mechanical properties of the Fe sample are studied. The results are supported by numerical modeling. The dislocation nucleation mechanism is proposed via a computational model. It is compared to high resolution electron backscatter diffraction (HR-EBSD) orientation image analysis, and shows information about the nanomechanical response of the Fe sample under external loads.

## 2. Experimental and computational methods

### 2.1. Experimental nanoindentation technique

Nanomechanical investigations were carried out by using a NanoTest Vantage system provided by Micro Materials Ltd. Measurements were performed at room temperature with a Berkovich-shaped diamond indenter tip. It is known that tip place a major role during low load nanoindentation [29]. Prior to the tests, the diamond area function (DAF) of the indenter was calibrated using fused silica with known mechanical properties. Indentations were performed in single force mode with a maximum load of 1.5 mN, which corresponds to 200 nm on pristine and 130 nm on irradiated samples. According to generally accepted nanoindentation principles, the plastic deformation regime induced during indentation, is 5–10 times greater than the penetration depth, depending on the material being tested [30]. This effect is less drastic in harder materials, with high yield strength. However in our studies, we adopted the most restrictive criterion to ensure that the material response comes from the irradiated layer, whose peak damage is located at a depth of around 1.3  $\mu\text{m}$ . The distance between indents was set at 10  $\mu\text{m}$ . For clarity, occasional faulty trials were manually excluded.

### 2.2. Electron backscatter diffraction (EBSD) analysis

A HR-EBSD analysis, in terms of local orientation gradients in grains deformed by nanoindentation, was performed using a Helios 5 UX (ThermoFisher Scientific) field emission scanning electron microscope operated at 25 kV and 6.4 nA current. A Kikuchi diffraction pattern was collected for each point at a camera resolution of  $640 \times 480$  pixels and a step size of 30 nm using EDAX Velocity Pro EBSD system. The orientation maps were analysed using OIM Analysis software with the application of a confidence index (CI) standardization routine and the filtering of the data with CI below 0.1.

### 2.3. Preparation of the pristine and irradiated material

The studied model material of high purity iron used in this work was cast by OCAS (Gent, Belgium) in an induction

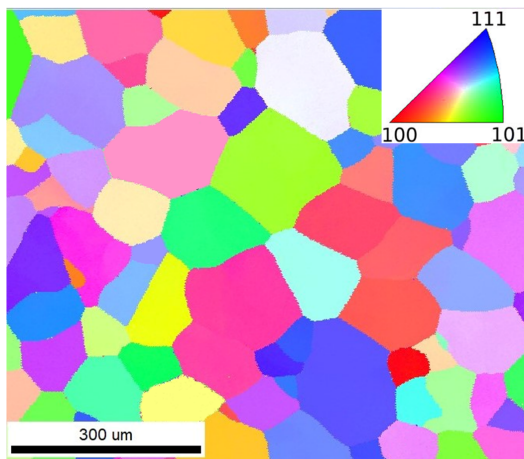
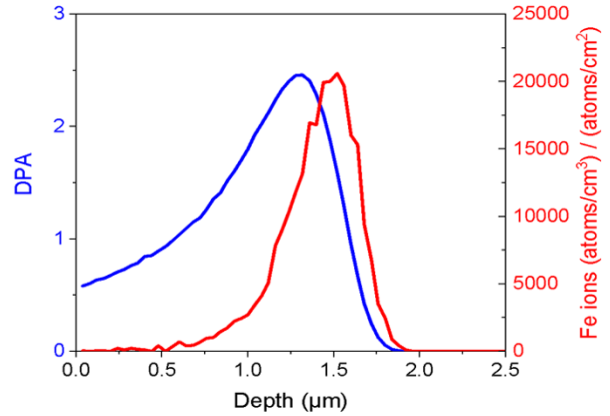
**Table 1**

Chemical composition of iron samples.

Element	C	Cr	Ni	Si	P	Al	Fe
Weight %	<0.005	0.002	0.007	0.001	0.003	0.013	Bal.

vacuum furnace by additive melting. The chemical composition is reported in Tab. 1. The studied model material was fabricated as a rolled plate with a final thickness of 10 mm. This was done by cutting a 50 mm × 125 mm × 250 mm piece from each lab cast. Then these pieces were introduced to the pre-heated furnace at 1200°C for 90 min. Following this step, hot rolling was performed (in 7 passes) until 10 mm was achieved. The hot rolling lasted for about 60 s, and the temperature of each element was approx. 930°C after the termination of the process. Afterward, cooling to room temperature in air was performed. The final dimensions of the sheets (measured in the rolling direction) were about 10 mm × 250 mm × 600 mm (height × width × length). The samples surface were mechanical polish at step-wise decreasing grain size of the polishing agent. One can observe in the EBSD IPF Z image (Fig. 1) that the studied specimens have large globular in shape grains with an average size of approximately 90 μm with fully ferritic microstructure and randomly distributed crystal orientation.

Ion irradiation was performed with the 3 MV tandem-tron accelerator located at the Ion Beam Center at HZDR Dresden. Fe<sup>2+</sup> ions with 5 MeV energy were implanted at 300°C into the sample. The temperature control was based on a thermo-couple placed on the backside of the sample, while the specimen was mounted on the heating target. The samples were scanned by a properly focused ion beam such that the irradiated area received a laterally uniform exposure corresponding to the respective predetermined target values. The ion flux was monitored continuously utilizing Faraday cups and integrated to obtain the ion fluence. The profiles of displacement damage in units of displacements per atom


**Figure 1:** (Color online) EBSD IPF Z image of the pristine Fe sample.

**Figure 2:** (Color online) Profiles of displacement damage (blue line) and concentration of injected interstitials (red line) for the 5 MeV Fe<sup>2+</sup>-ion irradiations, obtained by SRIM calculations.

(dpa) and injected interstitials per atom (ipa) were calculated using the SRIM binary collision code. This was done according to the recommendations given by Stoller et al.[31] using the quick Kinchin-Pease calculation and displacement energy of 40 eV. The respective profiles are plotted in Fig. 2.

## 2.4. Computational modeling

### 2.4.1. Molecular dynamics simulations framework

MD simulations is a used to describe the physical processes during nanoindentation testing, at an atomic level. For this, the Large-scale Atomic Molecular Massively Parallel Simulator (LAMMPS) [32] and interatomic potentials based on EAM method [33] were performed to describe Fe-Fe interaction. The modelling starts by the preparation of a single crystal [101] Fe sample with 11664000 Fe atoms in a (51.53, 54.66, 48.58) nm cell with density of 7.92 g/cm<sup>3</sup>, which agrees well with the experimental data. The size of the sample was chosen to be large enough for the anticipated propagation of dislocations along slip planes and dislocation dynamics throughout the BCC sample during the indentation process. Naturally, this requirement results in larger dimensions along the z-direction. Further, a process of energy optimization follows, and equilibration for 100 ps with a Langevin thermostat at room temperature. In order to emulate nanoindentation, the Fe sample is prepared by following the process explained in our previous work [7, 8, 34]. We utilize a repulsive imaginary (RI) rigid sphere as our indenter tip, with radius  $R = 10$  nm and a speed  $v = 20$  m/s, where  $v$  is chosen as positive for loading, and negative for unloading processes. Each calculation was performed for 125 ps with



a time step of  $\Delta t = 0.5$  fs. for a maximum indentation depth of 4.0 nm to avoid the influence of boundary layers of the material. This methodology was used in our previous works to model nanoindentation, in good agreement with experimental data [7, 8] Thus, the geometrically necessary dislocations (GNDs) are computed by using DXA method [35] implemented in OVITO [36].

### 2.4.2. 3D-DDD approach

The DDD approach applied in this paper exploits a coupling between a Dislocation Dynamics code [37] and a Finite Element (FE) solver [38] for consistently evaluating the dislocation stress field near the free surfaces. The coupling is based on the eigenstrain formalism [39], and implemented following the Discrete-Continuous Model (DCM) scheme [40, 14, 41, 15].

In the DCM, the stress field acting on dislocation segments is calculated by solving the Partial Differential (PD) equation of mechanical equilibrium. In this approach the plastic deformation is introduced in the constitutive equation by means of the eigenstrain formalism and a properly chosen regularization function [42]. This allows for the coupling with a FE numerical solver. The equilibrium equation to be solved thus become:

$$\begin{cases} -\nabla \vec{\sigma}(\vec{u}) = \vec{0} & \text{on } \Omega \setminus \partial\Omega \\ \vec{\sigma}(\vec{u}) = C(\vec{\epsilon}(\vec{u}) - \vec{\epsilon}^*) & \text{on } \Omega \setminus \partial\Omega \\ \vec{u} = \vec{0} & \text{on } \partial\Omega_D \\ \vec{\sigma} \cdot \vec{n} = \vec{0} & \text{on } \partial\Omega_N \\ \vec{\sigma} \cdot \vec{n} - k_{\text{pen}} \langle u - Z \rangle_+ = \vec{0} & \text{on } \partial\Omega_c \end{cases} \quad (1)$$

where  $\mathbf{u}$  is the unknown displacement field,  $\epsilon^*$  the eigenstrain, representing the plastic deformation,  $\Omega$  is the simulation volume and  $\partial\Omega$  its external boundary. The bottom boundary  $\partial\Omega_D$  is kept fixed by applying Dirichlet boundary conditions (zero displacement), while  $\partial\Omega_N$  is the top free surface with Neumann boundary conditions (zero normal stress). The last condition in Eq. (1), is applied to the contact region  $\partial\Omega_c$ . The constant  $k_{\text{pen}}$  is a penalization constant and the symbol  $\langle \cdot \rangle_+$  denotes the positive part of the argument. The function  $Z$  is used to define the outer surface of the indenter, modeled as the parabolic approximation of a sphere in this work.

In this way, boundary conditions for free surfaces of arbitrary geometry are fully taken into account when solving the PD system of Eqs. (1). Finally, the stress field resulting from the FE solution is used to compute forces that move dislocations at the  $N$ th + 1 time step, following an iterative process. It is important to highlight that, while the FE solver is in charge of computing the mechanical equilibrium, the DD code not only handles the movement of dislocation segments but it also manages potential reactions between them, modeling local interactions and recombinations. When two dislocation segments fall inside the regularized region their interaction is evaluated by means of the analytical expression derived in Ref. [42], consistently exploiting the same

regularization function  $\tilde{w}$ . Thus, the dynamics described by the DCM model is independent on the choice of the regularization thickness  $\tilde{h}$  [14].

For the purpose of this paper, simulation boxes of  $1 \mu\text{m}$  lateral sizes with lateral periodic boundary conditions were considered. The bottom boundary of the simulation cell is kept fixed while the top one is a free surface, as defined in Eq. (1). A distribution of pre-existing prismatic dislocation loops were placed under the indenter location to act as a trigger for the plastic deformation during nanoindentation. These loops were randomly selected between all possible glide systems for BCC Fe and with random positions in a small volume box (around 100 nm of lateral size) under the desired indenter location. Multiple simulations have been performed in order to confirm that details of the dislocation network at late indentation stages did not depend on the details of the initial prismatic loops distribution.

## 3. Results and discussion

The dislocation nucleation process plays a dominant role in the yield and subsequent plastic deformation of the material. To better understand the onset of plasticity by dislocation nucleation for the pristine case, the nanoindentation array was observed from the point of a specific grain. Figure 3a) shows an array of indents made on a grain with a preferential orientation of [101]. The test was performed on the pristine specimen. We analyzed the recorded HR-EBSD image and calculated the density of geometrically necessary dislocations (GNDs) on the surface near the indent. More GNDs are visible near the indenter tip and on one side,

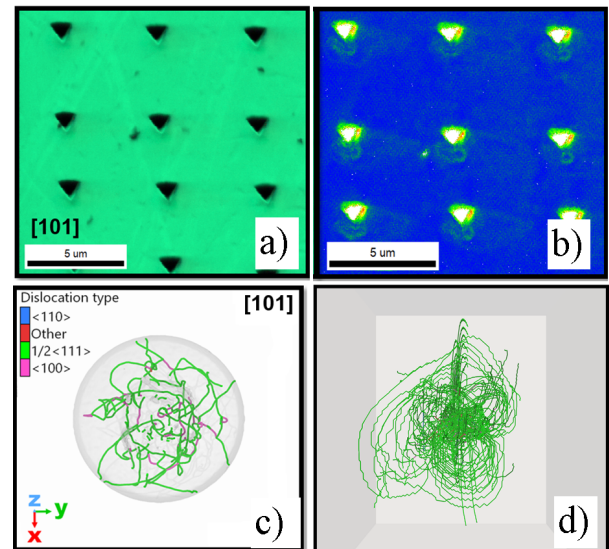


**Figure 3:** (Color online). a) EBSD map of the indentation array made within one grain with [101] orientation, b) GND density map of the indentation array, and c) calculated dislocation network at the maximum indentation depth calculated for the spherical indentation up to 4 nm depth; and d) 3D-DDD results for dislocation network following the coordinate tripo and dislocation color palette shown for the MD results.

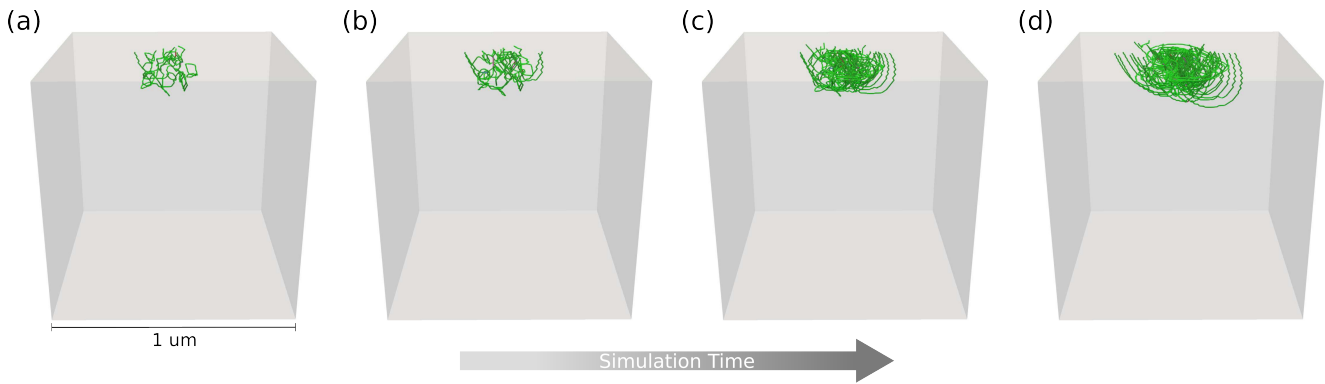


**Figure 4:** (Color online). Selected snapshots from a DDD simulation of nanoindentation of pure Fe in [101] directions. The initial configuration consists of randomly placed prismatic dislocation loops under the indenter as described in the text. The simulation times are 2 ns (a), 4 ns (b) 6 ns (c) and 8 ns (d). The maximum indentation depth shown in (d) corresponds to approximately 55 nm.

on the direction  $\{110\}$  slip plane. To better understand the mechanism of the loop formation, MD was carried out to simulate the indentation process. Fig. 3c) shows the developed dislocation types created in the [101] grain at the maximum indentation depth provide information of the dislocation forest underneath the tip. As expected,  $1/2\langle 111 \rangle$  loops are most common. In addition, the presence of  $\langle 110 \rangle$  and  $\langle 100 \rangle$  dislocation segments can be noticed. A very similar behavior has also been reproduced by means of DDD simulations, as reported in Fig. 3d). Here, the simulation box is much larger due to the computational advantages of DDD simulations and the maximum indentation depth simulated is much closer to the experimental one, around 55 nm. The dislocation network represents the same features observed in the MD simulation and in the experiments (Fig 3(b) and (c)) with the main network being formed by  $1/2\langle 111 \rangle$  dislocation loops. Some dislocation-dislocation reactions occur mainly forming  $\langle 100 \rangle$  dislocation segments and maintain their evolution as reported by DDD simulations (Fig. 5d).

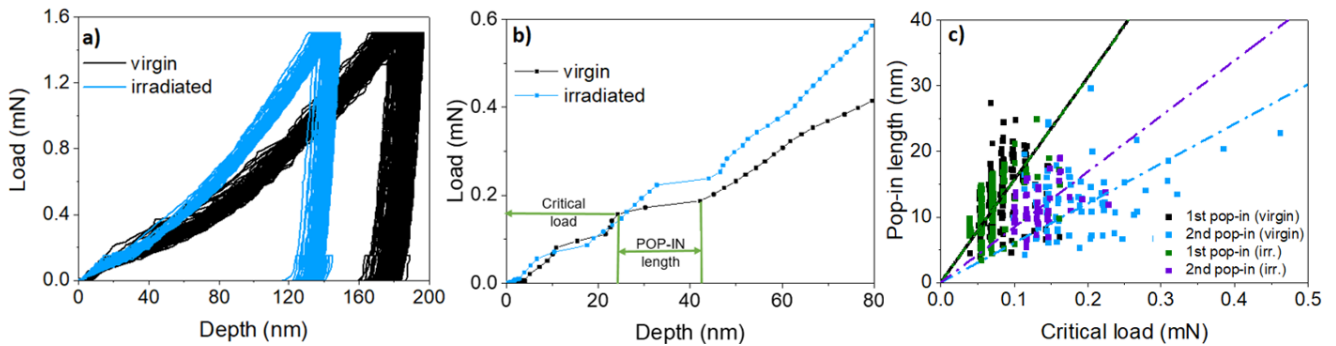
The temporal evolution of the dislocation microstructure can be better observed in Fig. 4 where selected snapshots from the loading process are extracted from a DDD simulation. As discussed in Section 2, the starting conditions of the DDD simulations performed here is a random distribution of prismatic loops placed under the indenter location. From this starting configuration the simulations evolve as shown for examples in Fig 4 (a)-(d). The dislocation loops rearrange under the influence of the indenter stress fields and start extending on their glide planes, multiplying and reacting in order to form the dislocation microstructure already described in Fig. 3. The maximum indentation depth achieved in this simulation is approximately 55 nm and the corresponding dislocation microstructures have already been reported in the top view of Fig. 3 (d).

Figure 5a) shows, recorded during indentation, load-indentation depth curves on pristine (black curves) and ion irradiated (blue curves) specimens. Indentations were performed with a constant load up to max 1.5 mN, resulting in deforming approx. 200 nm in the case of pristine and 130 nm

in the case of ion irradiated material. This load was chosen to assure the probing volume of the material, which does not extend below the irradiated region (even assuming a very constrained 1/10 criterion). Figure 5a) presents all recorded 200 indentation curves, hence, at first glance, the observed pop-in effect may be hidden.

Figure 5b) shows representative loading parts recorded during the indentation test. One can identify the occurrence of two clearly isolated pop-ins (with different magnitudes) in both cases. As described in the introduction section, the occurrence of a first pop-in can be attributed to the transition from purely elastic behavior to the onset of additional plastic deformation. All recorded curves show at least one pop-in event. This proves that the dislocation activation process followed by dislocation nucleation. This is a classical behavior for BCC metallic materials, and the recorded results are in full agreement with the experimental work of Ahn et al. [43] and numerical data provided by Biener et al. [44].

To quantify the occurring pop-in event, we calculated the number of pop-ins, length of the displacement, and critical load upon which this event commenced. This was done for both pristine and ion irradiated samples. Regardless of the state of the sample, a similar trend between the 1st and 2nd pop-ins has been observed. The first pop-in always occurs at a lower critical load and is statistically more significant than the second event. When considering only the first pop-in event, one can see that no difference between pristine and ion-irradiated material exists. In both cases, it requires approximately 10  $\mu\text{N}$  load to activate the event [20]. This proves that both samples have the same dislocation density and number of pre-existing mobile dislocations in the shear zone and have the same residual stress level at the surface after polishing. As demonstrated by Pöhl [45], polishing to high roughness level results in the development of isolated small pop-ins. This proved that local stress concentrations caused by surface discontinuity favor nucleation or activation of the pre-existing dislocations, which leads to the disappearance of the pop-in. We did not observe such phenomena in our case. Therefore, one can conclude that



**Figure 5:** (Color online) a) Experimentally recorded L–D curves of pristine (black line) and ion irradiated (blue line) pure Fe specimen. Indentations were performed up to the maximal load of 1.5 mN, which assured probing only radiation damage zone, b) representative loading part of the L–D curves marked with arrows, sudden displacement bursts represent the first and secondary pop-in effect recorded for both samples, and c) correlation between pop-in initiation load and length recorded for the first and secondary pop-in effect.

the roughness of the samples (and stress) are at the same level. However, one can see that a significant difference exists when comparing second pop-ins. Blue points represent the magnitude of the pop-in in the pristine sample, while purple points show the behavior of the ion irradiated sample. Statistically speaking, it is clearly seen that ion-irradiated samples shows a more consistent response. In addition, one can see that the first and second pop-ins recorded for pristine samples (see black and blue points on Fig. 5c) are slightly larger both in terms of the critical load necessary to activate the event and in pop-in length. It is known that in pure iron and BCC alloys generally, the mobility of pre-existing dislocations can be influenced by interstitial atoms such as carbon. One must remember that C is often introduced into the system during irradiation. In addition, the ion irradiation campaign was performed at 300°C, which is sufficient for C atoms to migrate and redistribute. Dissolved carbon atoms may diffuse into the stress fields of pre-existing dislocation, where they form the so-called Cottrell atmosphere, which results in dislocation pinning [46]. This impedes their mobility and can be observed as a much smaller amount of pop-ins and their lesser magnitude in ion irradiated material. Therefore, we believe that a significant reduction in pop-in magnitude is related partially to this effect. This is consistent with the work of Barnoush[47]. The second phenomenon responsible for lowering the magnitude of the pop-in is the presence of dislocation loops generated due to the development of radiation defects.

#### 4. Concluding remarks

In this work, we carried out a joint experimental, and multi-scale computational study of plastic deformation mechanisms of pristine and ion irradiated polycrystalline BCC iron through nanoindentation. For the pristine case, we characterized and described defect nucleation during nanomechanical testing and the evolution of geometrically necessary dislocations densities (GNDs) in [101] grain

indentation. To better understand the evolution during dislocation nucleation, we performed MD and 3D-DDD simulations, that showed the formation of GNDs, mainly with a Burgers vectors  $b = 1/2\langle 111 \rangle$ , in agreement with experiments. Furthermore, we investigated the pop-in behavior during nanoindentation. The analysis of L–D curves showed the occurrence of two sequential pop-ins in both cases studied (pristine, irradiated). The first pop-in is observed on both virgin and ion irradiated surfaces. In the case of the second pop-in, however, the irradiated sample required significantly higher stress for its activation, a phenomenon that may suggest that carbon was introduced into the material during ion irradiation at 300°C. At this temperature, carbon atoms may diffuse and form Cottrell atmospheres, resulting in dislocation pinning.

#### Acknowledgments

This work was supported by the Euratom research and training programme 2014–2018 under grant agreement no. 755039 (M4F project) and has been supported by the EURATOM Direct Actions. The research leading to these results was carried out in the frame of the Joint Programme on Nuclear Materials (JPNM) within the European Energy Research Alliance (EERA). This work is supported by the Ministry of Science and Higher Education through the Grant No 3908/H2020-Euratom/2018/2. We acknowledge support from the European Union Horizon 2020 research and innovation program under grant agreement no. 857470 and from the European Regional Development Fund via the Foundation for Polish Science International Research Agenda PLUS program grant No. MAB PLUS/2018/8. We acknowledge the computational resources provided by the High Performance Cluster at the National Centre for Nuclear Research in Poland. The ion irradiations were carried out at the Ion Beam Center at Helmholtz-Zentrum Dresden-Rossendorf (HZDR).

## CRedit authorship contribution statement

**K. Mulewska:** Writing Original draft preparation, Conceptualization of this study, Methodology, Investigation, Visualization, Data curation. **F. Rovaris:** Writing-Original draft preparation, Methodology, Software, Visualization, Data curation. **F. J. Dominguez-Gutierrez:** Writing-Original draft preparation, Methodology, Software, Visualization, Data curation. **W. Y. Huo:** Methodology, Writing - Review & Editing, Formal Analysis, Data curation. **D. Kalita:** Writing - Review & Editing, Data curation. **I. Jozwik:** Writing - Review & Editing, Formal analysis. **S. Papanikolaou:** Writing - Review & Editing, Data Curation, Formal analysis. **M. J. Alava:** Writing - Review & Editing, Data Curation. **L. Kurpaska:** Writing - Review & Editing, Conceptualization of this study, Investigation, Formal analysis. **J. Jagielski:** Writing - Review & Editing, Data Curation.

## References

- [1] C. A. Schuh, Nanoindentation studies of materials, *Materials Today* 9 (5) (2006) 32–40. doi:https://doi.org/10.1016/S1369-7021(06)71495-X.
- [2] A. Minor, S. S. Asif, Z. Shan, et al., A new view of the onset of plasticity during the nanoindentation of aluminium., *Nature materials* 5 (2006) 697.
- [3] J. K. Mason, A. C. Lund, C. A. Schuh, Determining the activation energy and volume for the onset of plasticity during nanoindentation, *Phys. Rev. B* 73 (2006) 054102. doi:10.1103/PhysRevB.73.054102. URL https://link.aps.org/doi/10.1103/PhysRevB.73.054102
- [4] P. Hosemann, D. Kiener, Y. Wang, S. A. Maloy, Issues to consider using nano indentation on shallow ion beam irradiated materials, *Journal of Nuclear Materials* 425 (1) (2012) 136.
- [5] D. Kiener, R. Pippan, C. Motz, H. Kreuzer, Microstructural evolution of the deformed volume beneath microindents in tungsten and copper, *Acta Materialia* 54 (10) (2006) 2801–2811.
- [6] I. Szlufarska, Atomistic simulations of nanoindentation, *Materials Today* 9 (5) (2006) 42–50.
- [7] F. Domínguez-Gutiérrez, S. Papanikolaou, A. Esfandiarpour, P. Sobkowicz, M. Alava, Nanoindentation of single crystalline mo: Atomistic defect nucleation and thermomechanical stability, *Materials Science and Engineering: A* 826 (2021) 141912. doi:https://doi.org/10.1016/j.msea.2021.141912.
- [8] L. Kurpaska, F. Dominguez-Gutierrez, Y. Zhang, K. Mulewska, H. Bei, W. Weber, A. Kosinska, W. Chrominski, I. Jozwik, R. Alvarez-Donado, S. Papanikolaou, J. Jagielski, M. Alava, Effects of fe atoms on hardening of a nickel matrix: Nanoindentation experiments and atom-scale numerical modeling, *Materials & Design* 217 (2022) 110639. doi:https://doi.org/10.1016/j.matdes.2022.110639.
- [9] G. Z. Voyiadjis, M. Yaghoobi, Review of nanoindentation size effect: Experiments and atomistic simulation, *Crystals* 7 (2017) 321. doi:https://doi.org/10.3390/cryst7100321.
- [10] M. Yaghoobi, G. Z. Voyiadjis, Effect of boundary conditions on the md simulation of nanoindentation, *Computational Materials Science* 95 (2014) 626–636. doi:https://doi.org/10.1016/j.commatsci.2014.08.013.
- [11] Y. Sato, S. Shinzato, T. Ohmura, T. Hatano, S. Ogata, Unique universal scaling in nanoindentation pop-ins, *Nature Communications* 11 (2020) 4177. doi:https://doi.org/10.1038/s41467-020-17918-7.
- [12] S. Lee, A. Vaid, J. Im, et al., In-situ observation of the initiation of plasticity by nucleation of prismatic dislocation loops., *Nat Commun* 11 (2020) 2367.
- [13] J. Varillas, J. Ocenasek, J. Torner, J. Alcalá, Unraveling deformation mechanisms around fcc and bcc nanocontacts through slip trace and pileup topography analyses, *Acta Materialia* 125 (2017) 431–441. doi:https://doi.org/10.1016/j.actamat.2016.11.067.
- [14] O. Jamond, R. Gatti, A. Roos, B. Devincere, Consistent formulation for the Discrete-Continuous Model: Improving complex dislocation dynamics simulations, *International Journal of Plasticity* 80 (2016) 19. doi:10.1016/j.ijplas.2015.12.011.
- [15] F. Rovaris, S. Papanikolaou, M. J. Alava, Effects of surface curvature and dislocation dynamics: Dynamical deformation mechanisms for uniaxial compression tests at the nanoscale, *Materials Science and Engineering: A* 846 (2022) 143270.
- [16] C. Xu, Y. Lu, Z. Fu, Y. Yang, In-situ tem characterization of the tensile deformation of ion-irradiated ht-ups steel at rt and 400 °c, *Journal of Nuclear Materials* 529 (2020) 151911. doi:https://doi.org/10.1016/j.jnucmat.2019.151911. URL https://www.sciencedirect.com/science/article/pii/S0022311519310979
- [17] S. Stangebye, Y. Zhang, S. Gupta, T. Zhu, O. Pierron, J. Kacher, Understanding and quantifying electron beam effects during in situ tem nanomechanical tensile testing on metal thin films, *Acta Materialia* 222 (2022) 117441. doi:https://doi.org/10.1016/j.actamat.2021.117441. URL https://www.sciencedirect.com/science/article/pii/S135964542100820X
- [18] J. Gagel, D. Weygand, P. Gumbsch, Formation of extended prismatic dislocation structures under indentation, *Acta Materialia* 111 (2016) 399.
- [19] S. Pathak, S. R. Kalidindi, Spherical nanoindentation stress-strain curves, *Materials Science and Engineering: R: Reports* 91 (2015) 1–36. doi:https://doi.org/10.1016/j.mser.2015.02.001.
- [20] L. Malerba, M. Caturba, E. Gaganidze, et al., Multiscale modelling for fusion and fission materials: The M4F project, *Nuclear Materials and Energy* 29 (2021) 101051.
- [21] A. Ruiz-Moreno, P. Hähner, Indentation size effects of ferritic/martensitic steels: A comparative experimental and modelling study, *Materials & Design* 145 (2018) 168–180.
- [22] K. Nordlund, S. Zinkle, A. Sand, et al., Improving atomic displacement and replacement calculations with physically realistic damage models, *Nat Commun* 9 (2018) 1084.
- [23] J. Henry, S. Maloy, Irradiation-resistant ferritic and martensitic steels as core materials for generation iv nuclear reactors, in: *Structural Materials for Generation IV Nuclear Reactors*, 2017, pp. 329–355. doi:https://doi.org/10.1016/B978-0-08-100906-2.00009-4.
- [24] A. Das, E. Altstadt, C. Kaden, G. Kapoor, S. Akhmadaliev, F. Bergner, Nanoindentation response of ion-irradiated fe, fe-cr alloys and ferritic-martensitic steel eurofer 97: The effect of ion energy., *Front. Mater.* 8 (2022) 811851.
- [25] J.-Y. Kim, J. R. Greer, Tensile and compressive behavior of gold and molybdenum single crystals at the nano-scale, *Acta Materialia* 57 (17) (2009) 5245–5253.
- [26] J. Marian, B. D. Wirth, J. M. Perlado, Mechanism of formation and growth of <100> interstitial loops in ferritic materials, *Phys. Rev. Lett.* 88 (2002) 255507.
- [27] S. L. Dudarev, R. Bullough, P. M. Derlet, Effect of the  $\alpha - \gamma$  phase transition on the stability of dislocation loops in bcc iron, *Phys. Rev. Lett.* 100 (2008) 135503.
- [28] J. Li, V. Vliet, K. Zhu, et al., Atomistic mechanisms governing elastic limit and incipient plasticity in crystals., *Nature* 418 (2002) 307.
- [29] A. Fischer-Cripps, Critical review of analysis and interpretation of nanoindentation test data, *Surface and Coatings Technology* 200 (14) (2006) 4153.
- [30] J. Chen, S. Bull, On the factors affecting the critical indenter penetration for measurement of coating hardness, *Vacuum* 83 (6) (2009) 911–920. doi:https://doi.org/10.1016/j.vacuum.2008.11.007. URL https://www.sciencedirect.com/science/article/pii/S0042207X08004892
- [31] R. Stoller, M. Toloczko, G. Was, A. Certain, S. Dwaraknath, F. Garner, On the use of srim for computing radiation damage exposure, *Nuclear Instruments and Methods in Physics Research Section B: Beam Interactions with Materials and Atoms* 310 (2013) 75–80.



- [32] A. P. Thompson, H. M. Aktulga, R. Berger, D. S. Bolintineanu, W. M. Brown, P. S. Crozier, P. J. in 't Veld, A. Kohlmeyer, S. G. Moore, T. D. Nguyen, R. Shan, M. J. Stevens, J. Tranchida, C. Trott, S. J. Plimpton, LAMMPS - a flexible simulation tool for particle-based materials modeling at the atomic, meso, and continuum scales, *Computer Physics Communications* 271 (2022) 108171. doi:<https://doi.org/10.1016/j.cpc.2021.108171>.
- [33] S. Eich, D. Beinke, G. Schmitz, Embedded-atom potential for an accurate thermodynamic description of the iron-chromium system, *Computational Materials Science* 104 (2015) 185. doi:<https://doi.org/10.1016/j.commatsci.2015.03.047>.  
URL <https://www.sciencedirect.com/science/article/pii/S0927025615002207>
- [34] F. J. Dominguez-Gutierrez, A. Ustrzycka, Q. Q. Xu, R. Alvarez-Donado, S. Papanikolaou, M. J. Alava 30 (8) (2022) 085010. doi:10.1088/1361-651X/ac9d54, [link].  
URL <https://dx.doi.org/10.1088/1361-651X/ac9d54>
- [35] A. Stukowski, Visualization and analysis of atomistic simulation data with OVITO-the Open Visualization Tool, *Modelling and simulation in materials science and engineering* 18 (1) (JAN 2010). doi:10.1088/0965-0393/18/1/015012.
- [36] A. Stukowski, V. V. Bulatov, A. Arsenlis, Automated identification and indexing of dislocations in crystal interfaces, *Modelling and Simulation in Materials Science and Engineering* 20 (8) (2012) 085007. doi:10.1088/0965-0393/20/8/085007.
- [37] B. Devincere, R. Madec, G. Monnet, S. Queyreau, R. Gatti, L. Kubin, Modeling crystal plasticity with dislocation dynamics simulations: The 'micromegas' code, in: O. Thomas, A. Ponchet, S. Forest (Eds.), *Mechanics of Nano-objects*, Presses de l'Ecole des Mines de Paris, Paris, 2011, p. 81–100.
- [38] A. Logg, K.-A. Mardal, G. Wells, *Automated Solution of Differential Equations by the Finite Element Method*, Springer, 2016.
- [39] T. Mura, *Micromechanics of defects in solids*, 2nd Edition, Vol. 3 of *Mechanics of Elastic and Inelastic Solids*, Dordrecht, 1987. doi:10.1007/978-94-009-3489-4.
- [40] A. Vattré, B. Devincere, F. Feyel, R. Gatti, S. Groh, O. Jamond, A. Roos, Modelling crystal plasticity by 3D dislocation dynamics and the finite element method: The Discrete-Continuous Model revisited, *Journal of the Mechanics and Physics of Solids* 63 (1) (2014) 491. doi:10.1016/j.jmps.2013.07.003.
- [41] F. Rovaris, F. Isa, R. Gatti, A. Jung, G. Isella, F. Montalenti, H. von Känel, Three-dimensional SiGe/Si heterostructures: Switching the dislocation sign by substrate under-etching, *Physical Review Materials* 1 (7) (2017) 073602. doi:10.1103/PhysRevMaterials.1.073602.  
URL <https://link.aps.org/doi/10.1103/PhysRevMaterials.1.073602>
- [42] W. Cai, A. Arsenlis, C. Weinberger, V. Bulatov, A Non-Singular Continuum Theory of Dislocations, *Journal of the Mechanics and Physics of Solids* 54 (3) (2006) 561. doi:10.1016/j.jmps.2005.09.005.  
URL <http://linkinghub.elsevier.com/retrieve/pii/S002250960500195X>
- [43] T.-H. Ahn, C.-S. Oh, K. Lee, E. P. George, H. N. Han, Relationship between yield point phenomena and the nanoindentation pop-in behavior of steel, *Journal of Materials Research* 27 (1) (2012) 39. doi:10.1557/jmr.2011.208.
- [44] M. M. Biener, J. Biener, A. M. Hodge, A. V. Hamza, Dislocation nucleation in bcc ta single crystals studied by nanoindentation, *Phys. Rev. B* 76 (2007) 165422.
- [45] F. Pöhl, Pop-in behavior and elastic-to-plastic transition of polycrystalline pure iron during sharp nanoindentation., *Sci Rep* 9 (2019) 15350.
- [46] K. Sekido, T. Ohmura, L. Zhang, T. Hara, K. Tsuzaki, The effect of interstitial carbon on the initiation of plastic deformation of steels, *Materials Science and Engineering: A* 530 (2011) 396–401. doi:<https://doi.org/10.1016/j.msea.2011.09.102>.  
URL <https://www.sciencedirect.com/science/article/pii/S0921509311010732>
- [47] A. Barnoush, Correlation between dislocation density and nanomechanical response during nanoindentation, *Acta Materialia* 60 (3) (2012) 1268–1277.